# PRACTICAL APPLICATION OF FAILURE MODELS TO PREDICT THE RESPONSE OF COMPOSITE STRUCTURES

R. Gutkin[1,*], S.T. Pinho[1]
[1]Department of Aeronautics, Imperial College London, UK
* Corresponding author(r.gutkin07@imperial.ac.uk)

**Keywords**: *failure, damage, finite element*

## 1 Introduction

Industrial structures present a large variety of geometries, stacking sequences, constraints and types of loadings. Such variety requires adequate meshing techniques, types of analysis and material models to be adopted at the different stages of design and development.

For composites structures, there is an additional need to account for failure and damage, as these may initiate at relatively low stress levels. It is therefore important to understand how damage modelling approaches are affected by the many factors listed above.

The present contribution focuses on the modelling techniques for failure in structures made of unidirectional carbon reinforced polymers. In particular, the added accuracy that can be expected from using advanced physically-based models versus simpler ones, as well as the added complexity costs, is investigated so that the former may be more widely used in industry. Three different damage models are investigated and compared. This manuscript presents the formulation and validation of the models as well as some basic examples highlighting differences in failure criteria, methods to handle damage propagation and type of solver used. Complementary examples dealing with meshing technique and interlaminar modelling will be presented during the oral presentation.

## 2 Failure Models

The failure models presented here are implemented following the same approach, based on three key elements: (i) a constitutive law, (ii) a set of failure criteria and (iii) a progressive damage model.

Constitutive laws (prior to failure onset) accounting for nonlinearity, effect of hydrostatic pressure [1,2] and damage [3] are available in the literature. These are not the focus of the present work, and the models developed here assume a linear elastic constitutive law prior to failure.

The failure criteria and progressive damage models are detailed in the next sections. The models are implemented as user material subroutines, for explicit and implicit schemes, to the FE package ABAQUS [4] for 3D solid elements.

In total, three different models are investigated:

1. an implicit model based on a physically-based failure criteria,
2. an explicit model based on a physically-based failure criteria (implemented in [2]),
3. an implicit model based on the maximum stress failure criteria.

### 2.1 Failure Criteria

Amongst the many criteria available in the literature, two of them are implemented and compared: (i) the simple, limit, criteria based on the maximum stress and (ii) a physically-based set of failure criteria.

#### *2.1.1 Maximum Stress Criteria*

For the 3D formulation of the maximum stress criteria, six different failure indices are defined: longitudinal direction (tension and compression), transverse direction (tension and compression), through the thickness (tension and compression) and failure in shear. The six indices are written in reduced form in Equation 1 and Equation 2

$$\frac{\langle \sigma_i \rangle_+}{\Sigma_T} + \frac{|\langle \sigma_i \rangle_-|}{\Sigma_C} \qquad \text{Equation 1}$$

with $i = \{1,2,3\}$ and

$$\text{if } \begin{cases} i=1 & \Sigma_T = X_T \quad \Sigma_C = X_C \\ i=2 & \Sigma_T = Y_T \quad \Sigma_C = Y_C \\ i=3 & \Sigma_T = Z_T \quad \Sigma_C = Z_C \end{cases}$$

and where $X_T$ and $X_C$ are the longitudinal tensile and compressive strengths, $Y_T$ and $Y_C$ are the transverse tensile and compressive strengths and $Z_T$ and $Z_C$ are

the through the thickness tensile and compressive strengths, respectively.

$$\frac{|\tau_{ij}|}{S} \qquad \text{Equation 2}$$

with $(i, j) = \{(12), (13), (23)\}$ and $S = S_{ij}$.
and where $S_{12}$ is the longitudinal shear strength, $S_{13}$ is the transverse shear strength and $S_{23}$ is the through the thickness shear strength (because of the transverse isotropy $S_{12} = S_{13}$).

*2.1.2 Physically-based Criteria*

The physically-based criteria involve five indices: fibre tension, fibre kinking, fibre splitting, matrix failure (as defined in [2]) and shear-driven fibre compressive failure [5].

**Matrix cracking** Equation 3

$$\sqrt{\left(\frac{\tau_T}{S_T^{is} - \eta_T \sigma_N}\right)^2 + \left(\frac{\tau_L}{S_L^{is} - \eta_L \sigma_N}\right)^2 + \left(\frac{\langle \sigma_N \rangle_+}{Y_T^{is}}\right)^2}$$

**Fibre tension** $(\sigma_1 \geq 0)$

$$\frac{\sigma_1}{X_T} \qquad \text{Equation 4}$$

**Shear-driven fibre compression** $\sigma_1 < 0$

$$\frac{\tau_N}{S_C} \qquad \text{Equation 5}$$

**Fibre kinking** if $\sigma_1 < -X_C/2$ or
**Matrix splitting** if $-X_C/2 < \sigma_1 < 0$ Equation 6

$$\sqrt{\left(\frac{\tau_{23}^m}{S_T^{is} - \eta_T \sigma_2^m}\right)^2 + \left(\frac{\tau_{12}^m}{S_L^{is} - \eta_L \sigma_2^m}\right)^2 + \left(\frac{\langle \sigma_2^m \rangle_+}{Y_T^{is}}\right)^2}$$

where $S_T^{is}$, $S_L^{is}$ and $Y_T^{is}$ are the transverse shear, longitudinal shear and transverse tensile in-situ strengths. The tractions on the fracture plane for the matrix and fibre modes, $\tau_{mn}$, $\tau_{nl}$, $\sigma_n$ and $\tau_{23}^m$, $\tau_{12}^m$ and $\sigma_2^m$ are defined in a general context in Fig.1 and in detail in [2].

**2.2 Progressive Damage**

Damage is often handled using damage mechanics, i.e. by introducing a damage variable representing the loss of load carrying area, which results in the definition of nominal stress as function of the effective stress:

$$\sigma = (1 - d)\ \bar{\sigma} \qquad \text{Equation 7}$$

*2.2.1 Damage evolution*

The evolution of the damage variable can be defined using a phenomenological approach [6] or based on cohesive law [7]. The second approach is chosen here. Once failure initiation is predicted, by one of the criteria described above, Equations 1 and 2 or Equations 3-6, the stresses on the elements considered are decreased according to a cohesive law, see Fig.2. The models are formulated using a smeared approach [7] so that the area under this cohesive law is equal to the fracture energy of the failure mode initiated divided by a characteristic dimension of the finite element. The shape of the curve can be adapted to account for R-curve effects [8], however only bi-linear cohesive laws are considered in the present work. The stress and strain defining the cohesive law (driving stress and strain) are the direct or shear stress and strain corresponding to the failure index activated for the model based on the maximum stress criteria, while for the models, explicit and implicit, based on the physically-based criteria, the driving stress and strain are as defined in [7].
For the different models implemented only two damage variables are introduced, namely one associated for fibre damage and one for matrix damage, and do not interact with each other. A regularisation scheme similar to the one in [4] is used.

*2.2.2 Effect of damage*

The effect of damage on the elastic constants of the material can be applied on the compliance tensor defined in the ply coordinate system or on the tractions acting on a given fracture plane (compliance tensor in the fracture plane coordinate system).

For the first approach, assuming transverse isotropy, the compliance tensor, **H** reads

$$\boldsymbol{H} = \begin{bmatrix} \frac{1}{(1-d_f)E_1} & -\frac{\nu_{12}}{E_1} & -\frac{\nu_{12}}{E_1} & & & \\ -\frac{\nu_{12}}{E_1} & \frac{1}{(1-d_m)E_2} & -\frac{\nu_{23}}{E_2} & & (0) & \\ -\frac{\nu_{12}}{E_1} & -\frac{\nu_{23}}{E_2} & \frac{1}{(1-d_m)E_2} & & & \\ & & & \frac{1}{(1-d_m)G_{12}} & & \\ & (0) & & & \frac{1}{(1-d_m)G_{12}} & \\ & & & & & \frac{1}{(1-d_m)G_{23}} \end{bmatrix}$$

Equation 8

This approach is preferred for the models implemented with the implicit scheme as the damaged stiffness matrix is required to define the Jacobian.

In the second approach, the effective stress tensor in the material coordinate system $\overline{\boldsymbol{\sigma}}_{123}$ is rotated to a coordinate system aligned with the fracture plane, as shown in Fig.1, thus defining

$$\overline{\boldsymbol{\sigma}}_{lmn} = \{\sigma_l \quad \sigma_m \quad \sigma_n \quad \tau_{lm} \quad \tau_{mn} \quad \tau_{nl}\}^T$$

Equation 9

The effective traction vector is degraded following Equation 7 and the nominal stresses expressed in the coordinate system aligned with the fracture plane are

$$\boldsymbol{\sigma}_{lmn} = \left\{\sigma_l \quad \sigma_m \quad \left(1 - d\frac{\langle\sigma_n\rangle_+}{\sigma_n}\right)\sigma_n \quad \tau_{lm} \quad (1-d)\tau_{mn} \quad (1-d)\tau_{nl}\right\}^T$$

Equation 10

This method is preferred for the explicit models as the nominal stress can be returned at the end of each increment.

## 3 Results

### 3.1 Failure Envelopes

To first validate the implementation of the models and illustrate the differences between them in predicting failure onset, failure envelopes for different load cases are generated. Forces in the directions investigated are proportionally applied onto a single element and the stress level is reported when a failure index reaches one. The failure envelopes are generated using a Python script interfacing with ABAQUS [4]. Such envelopes are shown in Fig.3 and Fig.4. The maximum stress criteria produce characteristic failure envelopes where the stress components do not interact with each other. Implicit and explicit models based on the physically-based criteria produce similar failure envelopes and match well the experimental data [9].

### 3.2 Failure Propagation

To illustrate the differences of the models in handling damage propagation, failure of a coupon loaded in transverse compression is presented. The FE model represents the gauge section of the coupon plus a portion of the grip, where damage propagation is deactivated. The material properties are given in Table 1. A normal distribution of transverse compressive strength (or through the thickness shear strength for the models based on the physically-based criteria) is assumed. The distribution is centered on the average value with a coefficient of variation of 10% as shown in Fig.5. The boundary conditions are also shown in Fig.5.

In transverse compression, it was observed in [7] that failure occurs at an angle of 53° to the loading direction. The two models based on the physically-based criteria capture well this feature as shown in Fig.6. The actual angle of the fracture is a direct consequence of the matrix failure criterion which uses that angle as input parameter; however, the localisation of fracture on that plane is a consequence of the progressive damage scheme.

The model based on the maximum stress criteria predicts a fracture angle orthogonal to the loading direction and does not reflect experimental findings.

The differences between the progressive damage schemes used, i.e. Equation 8 or Equation 10, is not significant in the case presented here in terms of the predicted failure pattern, even though the localisation, for a same level of applied displacement, is more pronounced in the explicit case. Because of this, the implicit model tends to bend out of plane rather than separating as in the explicit case.

### 3.3 Open Hole Tension

The models have in a first instance been applied to an Open Hole Tension (OHT) test case, for which the experimental procedure and results are reported in [10].

#### *3.3.1 Geometry and loading*

The geometry and boundary conditions applied to the models are shown in Fig.7a. For the implicit models an implicit dynamic scheme is used in order

to capture the load drop after failure. A small amount viscous regularisation is used to improve convergence ($\eta = 10^{-3}$ for the model based on the physically-based criteria and $\eta = 10^{-4}$ for the model based on the maximum stress)
Several meshing techniques and a mesh size sensitivity study have been done and the best compromise in terms of accuracy and CPU time is shown in Fig.7b.
The specimens are made of IM7/8552 (Table 1) with a stacking sequence of $[90/0/\pm45]_{3S}$ and the model is built on a ply by ply approach. Some models using cohesive contact to model interlaminar failure were investigated but are not presented here as the effect of delamination is minor for this stacking sequence.
Longitudinal strains are measured on the outer 90° ply at 3mm from the center line.

*3.3.2 Failure patterns*
In Fig.8, matrix damage patterns predicted by the models based on the physically-based criteria, both implicit and explicit, are very similar, with transverse cracking in the 90° plies and splits running in the ±45° plies. The plots are taken at the moment the strain in Fig.9 bifurcate. This happens earlier in the implicit model even though the extent of damage appears greater than in the explicit model. For the model based on the maximum stress criteria, the damage pattern in the 45° ply is similar to the other models but differs in the 90° ply with the crack branching at a short distance from the hole.

*3.3.3 Overall response*
The stress versus strain curves for the three models are shown in Fig.9. The models based on the physically-based criteria predict a failure stress in good agreement with the average experimental value.
The model based on the maximum stress criteria faces convergence difficulties at a strain of ~ $8.8\text{x}10^{-3}$, which are not resolved by adding regularisation.
For the models based on the physically-based criteria, the CPU time on 8CPUs varies from 15 mins for the explicit case to 46 mins for the implicit case.

## 4 Discussion and conclusion

The failure envelopes predicted by the different models show that physically-based criteria are better able to capture experimental trends.
Implicit and explicit formulations differ in the way the effect of damage can be included in the model and also in the way strain softening is handled (for instance viscous regularisation is not required in explicit). When similar failure criteria are used, the fracture angle and direction of damage predicted are similar in the cases studied here. The non-physically based model predicts relatively well failure patterns in in-plane cases but not the more complex through the thickness ones.
The explicit scheme does however show a more pronounced localisation of damage which can affect the global deformation of the model, Fig.6.
The explicit scheme shows also much better performance in terms of computational time. Furthermore, even though an explicit solution does not always exactly satisfy equilibrium (as in implicit), implicit models applied to highly non-linear problems typically require some form of viscous regularization and other artificial energy absorbing mechanisms.

**Acknowledgments**
EPSRC through the Knowledge Transfer Scheme and Airbus UK are gratefully acknowledged.

Table 1. Material properties
1- IM7/8552, 2-T300/914, 3-E-glass

| Property | Value | | | Source | | |
|---|---|---|---|---|---|---|
| Material system | 1 | 2 | 3 | 1 | 2 | 3 |
| $E_1$ (GPa) | 171 | 129 | 45.6 | [10] | [2] | |
| $E_2$ (GPa) | 9.08 | 5.6 | 16.2 | [10] | [2] | |
| $G_{12}$ (GPa) | 5.29 | 5.5 | 5.83 | [10] | [2] | |
| $\nu_{12}$ | 0.32 | 0.31 | 0.27 | [10] | [2] | |
| $X_T$ (MPa) | 2326 | 1378 | 1280 | [10] | [2] | |
| $X_C$ (MPa) | 1200 | 950 | 800 | [10] | [2] | |
| $Y_T$ (MPa) | 62 | 40 | 40 | [10] | [2] | |
| $Y_C$ (MPa) | 199 | 125 | 145 | [10] | [2] | |
| $S_L$ (MPa) | 92 | 97 | 73 | [10] | [2] | |
| $G_{IC}$ interlaminar ($kJ/m^2$) | 0.27 | | | [10] | | |
| $G_{IIC}$ interlaminar | 0.78 | | | [10] | | |

| | | |
|---|---|---|
| ($kJ/m^2$) | | |
| $G_{IC}^{FT}$ ($kJ/m^2$) | 97.8 | [2] |
| $G_{IC}^{FC}$ ($kJ/m^2$) | 106 | [2] |
| $G_{IC}^{MT}$ ($kJ/m^2$) | 0.25 | [2] |

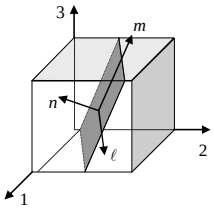


Fig.1. Coordinate system aligned with the crack [2].

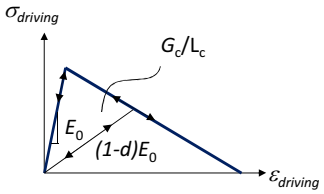


Fig.2. Bi-linear cohesive law.

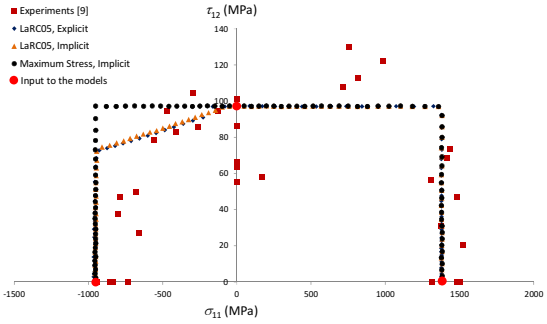


Fig.3. Failure envelopes for longitudinal loading combined with in-plane shear for the different models.

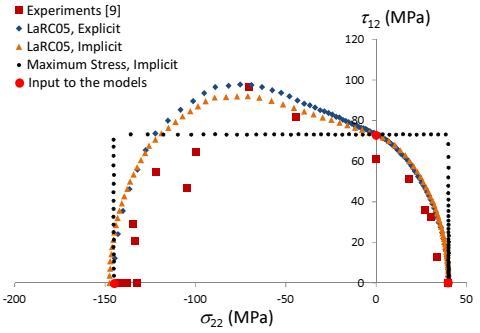


Fig.4. Failure envelopes for transverse loading combined with in-plane shear for the different models.

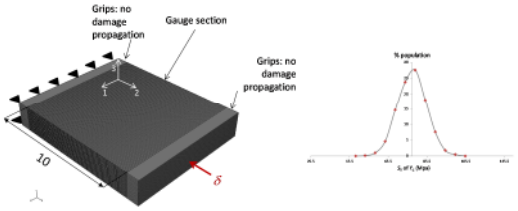


Fig.5. FE model for transverse compression specimen (dimension in mm)

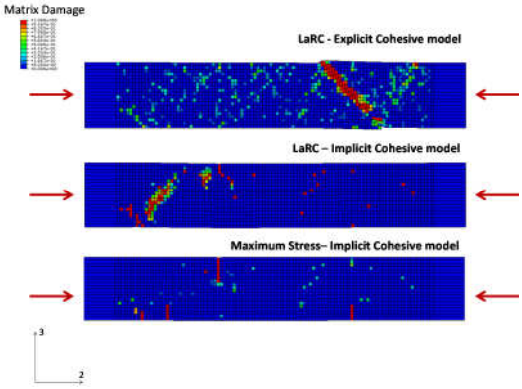


Fig.6. Transverse compressive failure

(a)

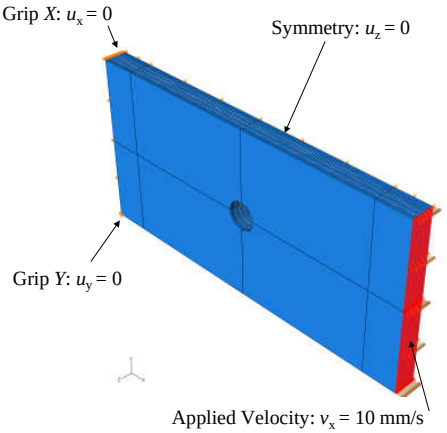


(b)

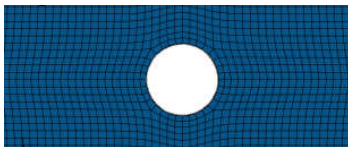

Fig.7. Open Hole Tension FE model (a) geometry and boundary conditions (b) mesh around the hole.

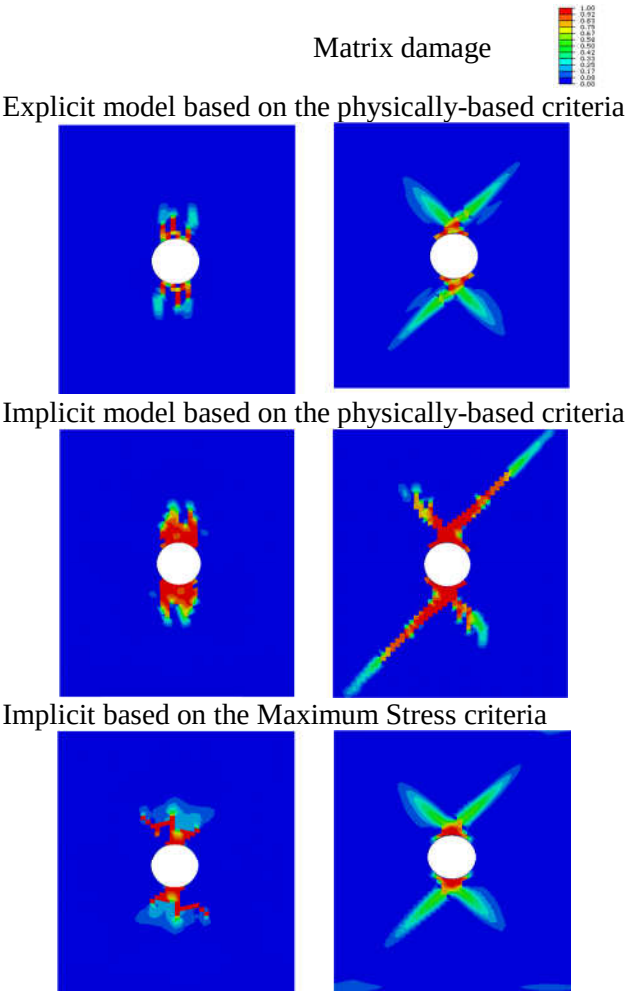


Fig.8. Matrix damage on outer 90° and inner 45° plies of an OHT for the three models.

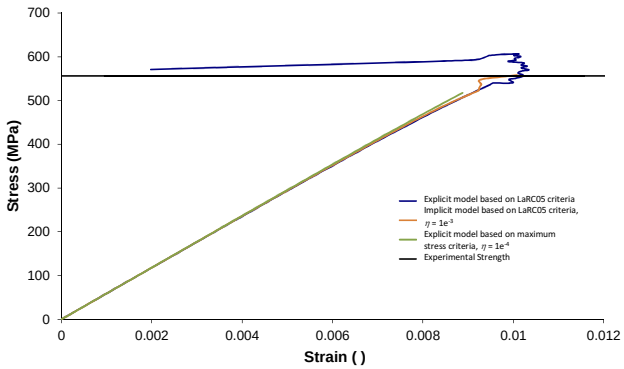


Fig.9. Predicted responses for an OHT test for three different failure models.

## References


[1] G.M. Vyas, S.T. Pinho, P. Robinson, "Constitutive modelling of fibre-reinforced composites with unidirectional plies using a plasticity-based approach". *Composites Science and Technology*, Vol. 71,pp 1068-1074, 2011.

[2] S. T. Pinho, R. Darvizeh, P. Robinson, C. Schuecker and P. P. Camanho, "Material and structural response of polymer-matrix fibre-reinforced composites". *Composites Science and Technology* 2008; accepted for publication. (Special issue on Second World Wide Failure Exercise).

[3] P. Maimí, P.P. Camanho, J.A. Mayugo, A. Turon, "Matrix cracking and delamination in laminated composites. Part I: Ply constitutive law, first ply failure and onset of delamination". *Mechanics of Materials*, Vol. 43, pp 169-185, 2011.

[4] Abaqus, Hibbit and Karlson and Sorensen Inc., User's manual – version 6.9-EF, 2009.

[5] R. Gutkin, S.T. Pinho, P. Robinson, P.T. Curtis , "On the transition from shear-driven fibre compressive failure to fibre kinking in notched CFRP laminates under longitudinal compression", Composites *Science and Technology*, Vol. 70, pp 1223-1231, 2010.

[6] C. Schuecker, H.E. Pettermann, "Constitutive ply damage modeling, FEM implementation, and analyses of laminated structures", *Computers and Structures*, Vol. 86, pp 908–918, 2008.

[7] S.T. Pinho, L. Iannucci, P. Robinson, "Physically based failure models and criteria for laminated fibre-reinforced composites with emphasis on fibre kinking. Part II: FE implementation", *Composites Part A: Applied Science and Manufacturing*, Vol. 37, pp 766-777, 2006.

[8] R. Gutkin, M.L. Laffan, S.T. Pinho, P. Robinson, P.T. Curtis, "Modelling the R-curve effect and its specimen-dependence", *International Journal of Solids and Structures*, Vol. 48, pp 1767-1777, 2011.

[9] P. D. Soden, M. J. Hinton, A. S. Kaddour, "Biaxial test results for strength and deformation of a range of E-glass and carbon fibre reinforced composite laminates: failure exercise benchmark data", *Composites Science and Technology*, Vol. 62, pp 1489-1514, 2002.

[10] P.P. Camanho, P. Maimí and C.G. Dávila,"Prediction of size effects in notched laminates using continuum damage mechanics". *Composites Science and Technology*, Vol. 67,pp 2715-2727, 2007.